



Formation evaluation and reservoir potential of the Middle Miocene syn-rift Hammam Faraun Member from the offshore Esh El Mellaha area, southern Gulf of Suez, Egypt

Sherif Farouk¹ · Souvik Sen² · Ahmed K. El-Behery³ · Fayez Ahmad⁴ · Khaled Al-Kahtany⁵

Received: 17 May 2024 / Accepted: 25 June 2024

© The Author(s), under exclusive licence to Springer Nature B.V. 2024

Abstract

This study presents an integrated formation evaluation of the Middle Miocene syn-rift sandstones of the Hammam Faraun Member from the southern Gulf of Suez. Core data, XRD, wireline logs, and gas chromatography data have been utilized to assess the reservoir characteristics. Three lithofacies are identified from the cored intervals: (i) fine to medium-grained massive sandstone (F-1), (ii) low-angle cross-bedded fine-grained sandstone (F-2); and (iii) coarse to very coarse-grained massive sandstone (F-3). The dominantly massive nature of the sand units with sharp erosive base and bottom rip-up clasts strongly indicates a high energy channel or fan deposit. XRD analysis reveals quartz and feldspar to be the dominant constituents of this calcareous arkose. Montmorillonite and kaolinite are the major clay phases, along with minor illite. Routine core analysis of a total of 168 core plugs indicates meso- to megaporous sandstones with porosity up to 28% and Kh up to 1171 mD. Permeability anisotropy analysis exhibits the dominance of primary depositional fabric and isotropic pores. Wireline log analysis yielded shale volume < 0.2 v/v, porosity ~ 0.18–0.24 v/v, and water saturation ~ 0.33–0.49 v/v. Various gas ratios (wetness, balance, character, and oil indicator ratio) estimated from the chromatograph data indicate the presence of liquid hydrocarbons within the studied reservoirs. The study concludes excellent reservoir properties in the Hammam Faraun clastic intervals of the Esh El Mellaha area.

Highlights

- Hammam Faraun reservoirs consist of meso-megaporous calcareous arkose.
- Massive sands with sharp erosive base and bottom rip-up clasts indicates a high energy tidal deposit.
- Wireline logs indicate poor shale volume and considerable hydrocarbon saturation.
- Gas chromatography data confirms the presence of liquid hydrocarbon.

Keywords Routine core analysis · Petrophysics · Gas chromatography · Hammam Faraun · Southern Gulf of Suez

✉ Sherif Farouk
geo.sherif@hotmail.com

¹ Exploration Department, Egyptian Petroleum Research Institute (EPRI), 1 Ahmed El-Zomor Street, Nasr City, Cairo 11727, Egypt

² Reservoir Technical Services (RTS), Baker Hughes, Mumbai, Maharashtra, India

³ South Valley Egyptian Petroleum Holding Company, Nasser City, Cairo, Egypt

⁴ Prince El-Hassan Bin Talal Faculty of Natural Resources and Environment, Department of Earth and Environmental Sciences, The Hashemite University, Zarqa, Jordan

⁵ Geology and Geophysics Department, College of Science, King Saud University, King Saud, Saudi Arabia

Introduction

The Gulf of Suez (GOS) in Egypt is one of the most prolific hydrocarbon-producing basins in northern Africa. It is an aborted continental rift basin, however, presently active, and the footwalls of several major extensional faults are still rising to this day (Bosworth and Durocher 2017). Almost one-fifth of the cumulative production of the GOS comes from the Middle Miocene reservoirs (Patton et al. 1994). GOS produced 54.5 million barrels of oil in 2020, which shows a 3.8% decline from the previous year's production due to the natural decline of the mature fields (Hussein et al. 2020). However, GOS remained the upstream activity

hotspot, along with the Nile Delta and onshore Western Desert regions. The recently discovered Al Wasl field, one of the biggest in the last 20 years, will start commercial production in 2024. It has brought attention and renewed interest to the upstream community about the future GOS potential. Our study focuses on the southern GOS. Elleboudy et al. (2011) estimated around 4.764 barrels of oil equivalent of ultimate recoverable resources and 2.614 barrels of oil equivalent of remaining undiscovered hydrocarbons in the southern Gulf of Suez. Recent hydrocarbon discoveries in the pre-rift Nubia and early Miocene Nukhul intervals of the Geisum and Tawila West Concessions in the southern GOS indicate the promising future of this region. Our study area, Esh El Mellaha, is close to these discoveries and commercially produces from the Matulla and Nukhul formations (Omran et al. 2022a).

Previous studies from the southern GOS discussed the structural geology (Meshref et al. 1995; Omran and El Sharawy 2014; Nabawy and El Sharawy 2015; Maestrelli et al. 2020; Van Dijk et al. 2020), in-situ stress state (Bosworth and Durocher 2017; Radwan et al. 2021), Miocene sequence stratigraphy (Ramzy et al. 1996; El-Naby et al. 2016), source rock evaluation of Duwi, Kareem and Rudeis formations (El Sharawy and Gaafar 2012; El Nady and Mohamed., 2016), petrophysical analysis of Upper Cretaceous successions (El Sharawy and Nabawy 2016; Omran et al. 2022b; Selim and Sarhan 2024), reservoir characterization of Kareem Formation (Farouk et al. 2022a; Hussein et al., 2024), seismic interpretation and reservoir evaluation of the Nubia, Nukhul and Rudies formations (Omran et al. 2022b), geostatic modeling and reserve estimation of the Middle Miocene reservoirs (Amer et al. 2023). The Esh El Mellaha area of the southern Gulf of Suez is less discussed. Only two publications are available from this region. Elbahrawy et al. (2023) studied the Upper Cretaceous Matulla reservoirs of the Esh El Mellaha area by integrating the seismic interpretation and wireline log analysis. Omran et al. (2022a) interpreted the well logs and characterized the Rudeis, Nukhul, Matulla, Nubia and basement reservoir intervals from the onshore West Esh El Mellaha area. However, a detailed formation evaluation of the Middle Miocene syn-rift Hammam Faraun Member of the Belayim Formation lacks in the literature which sets the premise of this work. We have integrated core data, wireline logs and mud-logging data to characterize the mentioned reservoir. The primary objectives of this study are to: (i) infer lithofacies from core-based observations, (ii) bulk mineralogy and clay fraction from X-ray diffraction (XRD), (iii) porosity, permeability and permeability anisotropy analysis from routine core analysis (RCA), (iv) quantitative petrophysical interpretation from wireline logs and (v) gas chromatography data analysis and infer possible hydrocarbon phases based

on various gas ratio interpretation. The results are discussed, and inferences are drawn on depositional environment and reservoir quality.

Geological settings

The GOS rift basin was formed during the Upper Oligocene to Lower Miocene and continued until the Upper Miocene (Bosworth et al. 2020). The rift basin, bounded by NW-SE faults (Fig. 1), was created by a NE to NNE extension during the separation of the Arabian and African plates (Moustafa 1993; Patton et al. 1994; Younes and McClay 2002). The maximum horizontal stress azimuth was inferred as N150°E based on the drilling induced tensile failures reported from the Hilal oil field of southern GOS (Radwan et al. 2021). The southern Suez rift ends by creating a triple junction with Gulf of Aqaba and Red Sea rifting. Meshref (1990) subdivided the Suez rift basin into various structural provinces based on dip variations within large fault blocks constituting eroded horsts and deep grabens. This study focuses on the offshore Esh El Mellaha area, located on the southern offshore part of the GOS (Fig. 1a). Elbahrawy et al. (2023) interpreted the structural setting of this area by integrating seismic and remote sensing datasets.

The Precambrian to recent stratigraphy of the study area is divided into three mega-units (Said 1990): the Precambrian to Eocene pre-rift unit, ii) the Miocene syn-rift unit and iii) the Pliocene-recent post-rift unit. This study focuses on the Miocene syn-rift interval, which unconformably lies above the pre-rift sediments. A stratigraphic chart of the Miocene interval is presented in Fig. 2 (Alsharhan 2003). Distinct lithological variations are observed in the two major groups of the Miocene interval. The Lower to Middle Miocene Gharandal Group is devoid of any major anhydrite and consists of Lower Miocene Nukhul, Rudeis formations, and Middle Miocene Kareem Formation. These are characterized by mixed clastic and carbonate lithologies (Elmaadawy 2020; Elmaadawy et al. 2021). The Middle Miocene Ras Mallab Group consists of Belayim, South Gharib and Zeit formations. The Belayim Formation is divided in four members: Baba and Feiran are anhydrite dominated, Sidri is sandstone dominated and Hammam Faraun exhibits mixed lithologies (Alsharhan 2003). The South Gharib and Zeit formations are composed mainly of salt and anhydrites. The vertical and lateral facies variations of the syn-depositional Miocene units are largely controlled by the structural framework of the southern Gulf of Suez guided by the diapiric structure of South Gharib Formation (El-Naby et al. 2016). The marls of the Rudeis and Hammam Faraun formations along with the Kareem shales are the potential source rocks (El Nady and Mohamed., 2016). The syn-rift unit hosts

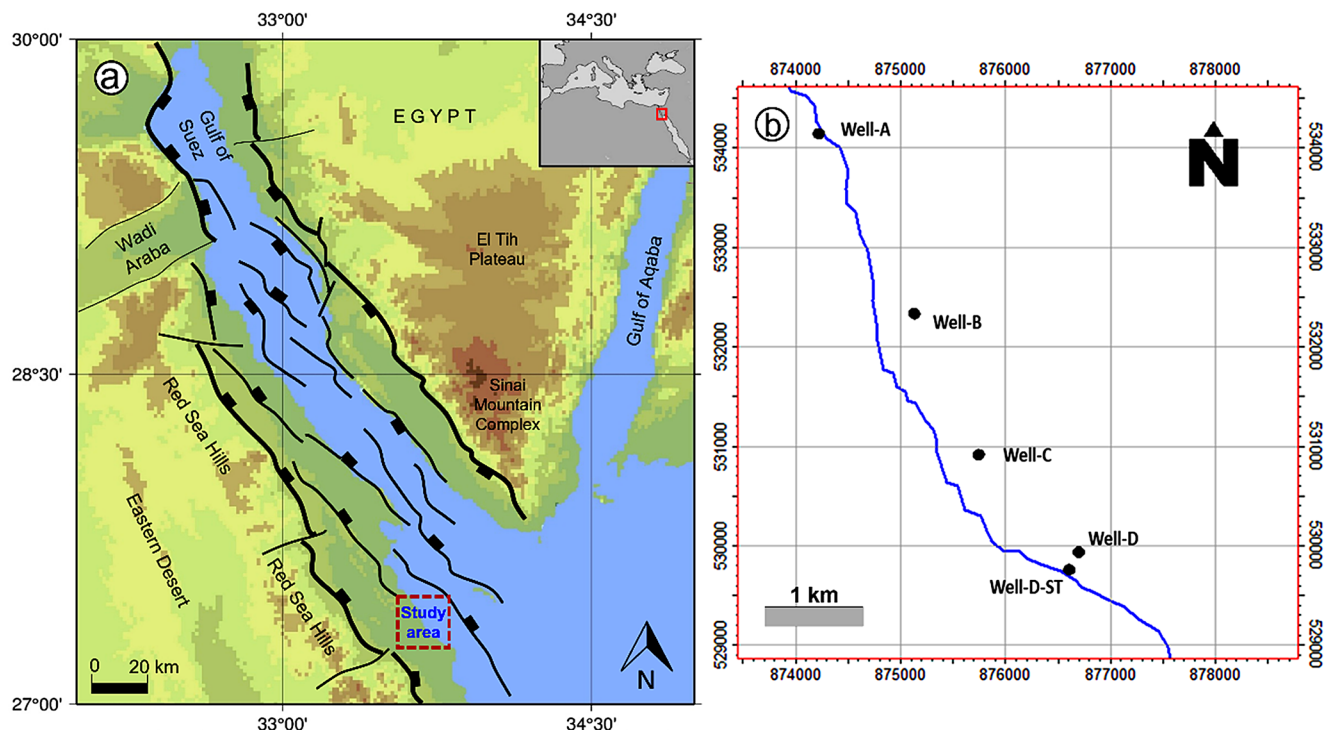


Fig. 1 (a) Location of the study area - offshore Esh El Mellaha, southern Gulf of Suez, as marked by red square along with the major faults. The base map is prepared by using CASMI, a visualization tool for the

World Stress Map (WSM) database accessed by the online interface CASMO (Heidbach et al. 2010). (b) location of the five studied wells in the study area

multiple sandstone and limestone reservoirs within Nukhul, Rudeis, Sidri, and Hammam Faraun (Amer et al. 2023; Selim and Sarhan 2024). The Middle Miocene South Gharib and Zeit formations provided a regional seal to the underlying syn-rift reservoirs (Alsharhan 2003).

Data and methods

We have studied the Middle Miocene syn-rift Hammam Faraun sandstone reservoir of the Belayim Formation from five wells drilled in the offshore Esh El Mellaha, southern Gulf of Suez. The well names are Well-A, Well-B, Well-C, Well-D and Well-D ST. The well locations are presented in Fig. 1b. All these wells were drilled to the base of the Belayim Formation. Conventional cores were acquired in three wells: Well-B, Well-C and Well-D ST, which were studied for lithofacies analysis. XRD analysis were performed on three samples from Well-B which provided bulk rock composition as well as clay mineralogy. Routine core analysis (RCA) was performed on the 15 plug samples of Well-B, 95 samples of Well-C and 58 samples from Well-D ST. Helium porosity and horizontal permeability (Kh) measurements were available from 153 samples of Well-C and Well-D ST. Only porosity measurements were available from Well-B samples, while vertical permeability (Kv)

was measured only on the Well-C samples. Based on the Kh and Kv measurements in Well-C, permeability anisotropy (λ_k) was estimated (Nabawy and Al-Azazi 2015a; Nabawy 2018):

$$\lambda_k = \sqrt{\frac{K_h}{K_v}} \tag{1}$$

Wireline logs were acquired which covered the target reservoir interval in all the wells. Available wireline logs include gamma ray (GR), resistivity (RLA5 and RXOZ), bulk density (RHOB), neutron porosity (NPHI) and compressional acoustic slowness (DT). A well-log correlation panel (based on the gamma-ray log) is presented in Fig. 3. A cross-plot between RHOB and NPHI was prepared to identify the lithological composition of the studied interval (Asquith and Krygowski 2004). To infer the mineralogical composition, we utilized M-N cross-plot based on RHOB, NPHI and DT. ‘M’ and ‘N’ are defined as:

$$M = \left(\frac{DT_f - DT}{RHOB - RHOB_f} \right) * 0.01 \tag{2}$$

$$N = \frac{NPHI_f - NPHI}{RHOB - RHOB_f} \tag{3}$$

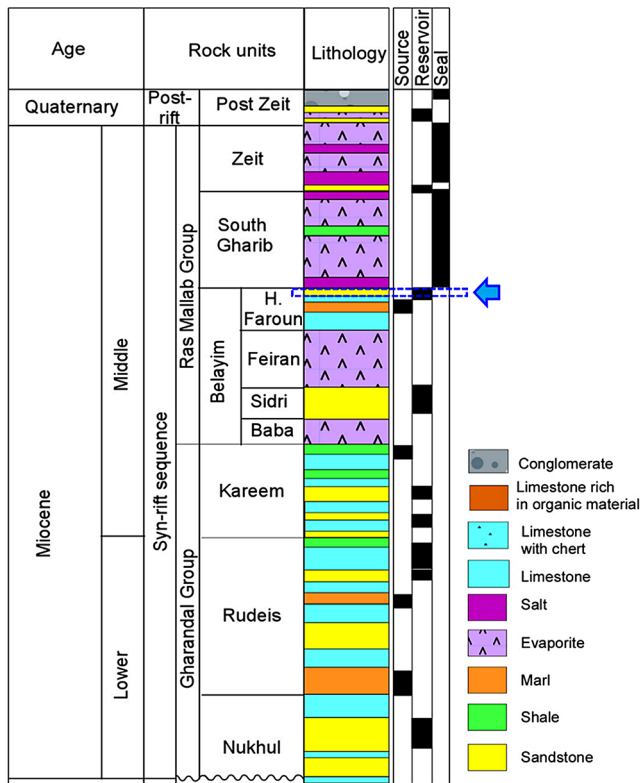


Fig. 2 Miocene lithostratigraphic succession of the study area - offshore Esh El Mellaha, southern Gulf of Suez (Alsharhan 2003). The studied interval, i.e., Middle Miocene syn-rift Hammam Faraun Member of the Belayim Formation is marked by blue rectangle and arrow

Where DTf is the slowness of the formation fluid and RHOBf is the formation fluid density. To infer the matrix composition, a cross-plot was prepared using apparent matrix density (RHOMAA) and apparent matrix volumetric photoelectric factor (UMAA). Key petrophysical parameters were estimated utilizing the wireline logs, which include shale volume (Vsh), total porosity (PHIT), effective porosity (PHIE), water saturation (Sw) and bulk volume of water (BVW). Vsh was inferred from the gamma-ray log; PHIT and PHIE were estimated from RHOB, NPHI and Vsh (Asquith and Gibson 1982). The Sw was estimated by the Indonesian model (Poupon and Leveaux 1971):

$$Sw = \left\{ \frac{\sqrt{\frac{1}{R}}}{\left\{ \left(\frac{Vsh^{1-0.5Vsh}}{\sqrt{Rsh}} \right) + \sqrt{\frac{\phi_e m}{aRw}} \right\}} \right\}^{\frac{2}{n}} \quad (4)$$

Where, R=deep resistivity log response, Rsh=shale resistivity; Rw=resistivity of the connate water, considered as 0.028 ohmm; ‘a’ is tortuosity factor (considered a=1); ‘m’ is cementation exponent and ‘n’ is saturation exponent. We assumed m=2 and n=2. Net pay interval was distinguished

based on the petrophysical cut offs of porosity=0.1 v/v, Vsh=0.35 v/v, and Sw=0.5 v/v, as commonly reported from Gulf of Suez (Ali et al. 2022). Upscaled log petrophysical properties are populated across the field to infer the lateral distribution of reservoir parameters.

Along with the core analysis and wireline log-based quantitative petrophysical assessment, the gas data from mudlogging services were also studied to infer the possible hydrocarbon characteristics. Gas chromatography data was studied from three wells, Well-C and Well-D. Based on the total gas and chromatographs (C1 to C5), following wetness ratio (Wh), balance ratio (Bh), gas character ratio (Ch) and oil indicator ratio (OI) were estimated (Haworth et al. 1985; Pierson 2017):

$$Wh = \left[\frac{C2 + C3 + C4 + C5}{C1 + C2 + C3 + C4 + C5} \right] * 100 \quad (5)$$

$$Bh = \frac{C1 + C2}{C3 + C4 + C5} \quad (6)$$

$$Ch = \frac{C4 + C5}{C3} \quad (7)$$

$$OI = \left[\frac{C3 + C4}{C1} \right] * 100 \quad (8)$$

Based on the value ranges of the estimated gas ratios, reservoir fluid types are inferred (Haworth et al. 1985; Mode et al. 2014; Pierson 2017).

Esh El Mellaha.

Results

Lithofacies and XRD analysis

Conventional cores recovered from Well-B, Well-C and Well-D ST were studied for lithofacies analysis (Fig. 4). Three distinct lithofacies were identified: (i) fine to medium-grained massive sandstone (F-1), (ii) low-angle cross-bedded fine-grained sandstone (F-2) and (iii) coarse to very coarse-grained massive sandstone (F-3). Deposition of low-angle crossbed lithofacies (i.e., F-2) usually indicates a hydrodynamic condition between upper plane bed and antidune formation, therefore representing a subcritical to critical flow transition. F-1 and F-3 are devoid of any primary sedimentary structures. F-3 exhibits an erosive base, rip-up clasts, and sharp contact with the underlying F-2 (Fig. 4).

The XRD measurements were available only from three samples of Well-B which provided information about the bulk rock composition as well as clay mineralogy. Results

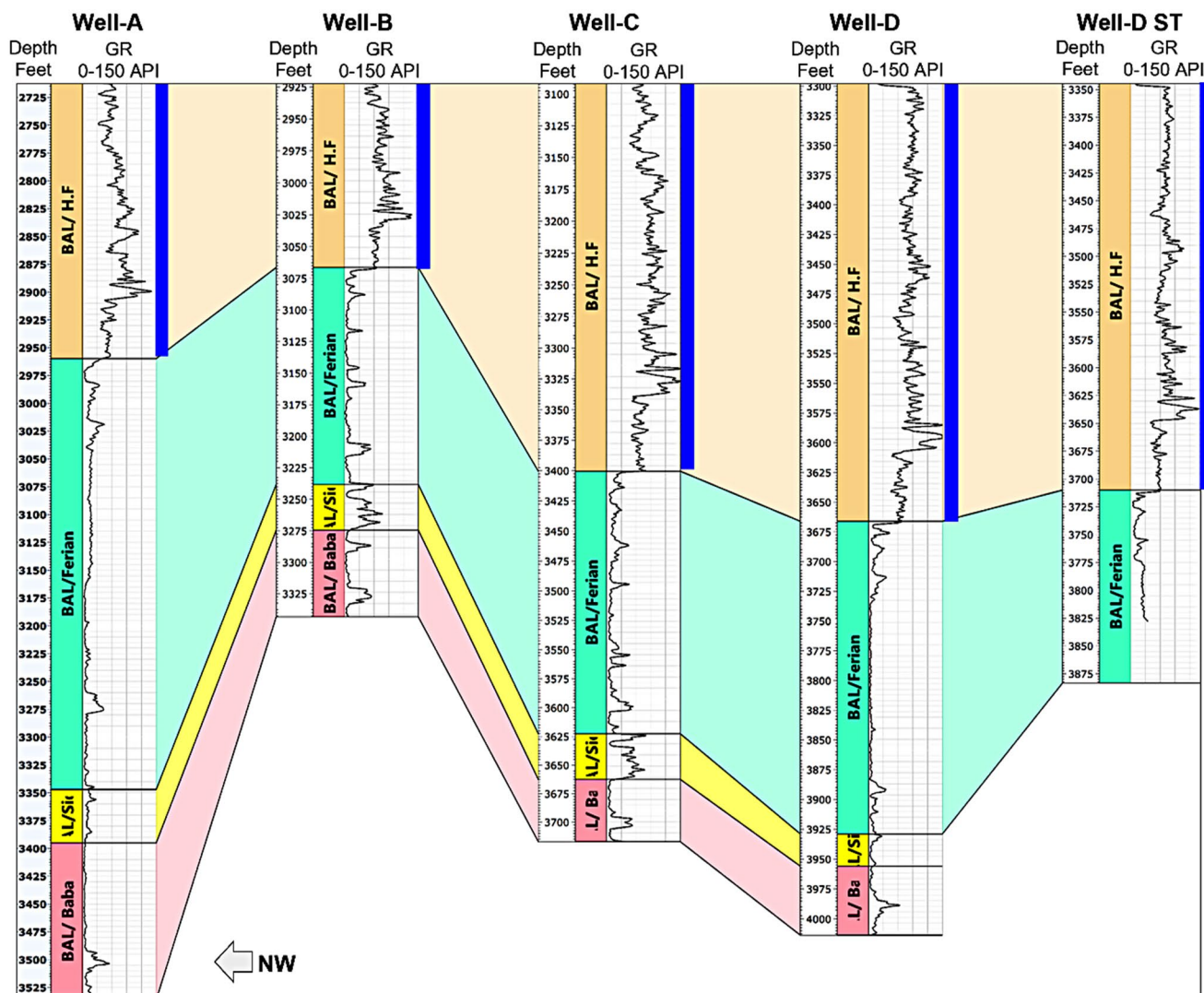


Fig. 3 Well log correlation panel using the five studied wells in the offshore Esh El Mellaha, southern Gulf of Suez. The studied interval ‘BAL/H.F.’ denotes the studied Middle Miocene syn-rift Hammam Faraun Member of the Belayim Formation, denoted by blue bar in each well

are presented in Fig. 5. These samples were recovered from the F-2 lithofacies. It indicates quartz and feldspar to be the dominant mineral constituents of the Hammam Faraun clastic intervals (Fig. 5a). Quartz abundance varies between 51 and 65%, while feldspar ranges between 30 and 38%. Clay content varies between 4 and 7%. Two of the samples exhibited minor carbonates, around 5%. Since the point count data is unavailable from the petrographic thin section study, we considered the XRD-based relative abundance of quartz and feldspar for sandstone classification which indicates that the studied Hammam Faraun interval is Arkose in nature, as per Folk’s (1980) classification. Clay fraction data is presented in Fig. 5b indicating the presence of montmorillonite as the dominant clay phase with abundance ranging between 53 and 85%. Kaolinite content ranges between 11

and 33% and illite is the least abundant clay fraction ranging between 4 and 14%.

Routine core analysis

RCA indicates a porosity range of 13–28% in the Hammam Faraun interval (Fig. 6a) (14.5–25.8% in Well-B, 12.9–28.3% in Well-C and 13–28% in Well-D ST). Kh measurements in Well-C range between 0.6 and 222 mD, while the Well-D ST exhibits a higher Kh range of 2.7–1171 mD (Fig. 6a). Majority of the Well-C measurements are indicative of mesoporosity ($0.5 \mu\text{m} < R_{35} < 2 \mu\text{m}$) with some macroporosity ($2 \mu\text{m} < R_{35} < 10 \mu\text{m}$) (Fig. 6a). Well-D ST measurements indicate dominantly macroporosity with some megaporosity ($R_{35} > 10 \mu\text{m}$) (Fig. 6a). Kv measurements in Well-C exhibits a wide range between 0.16 and

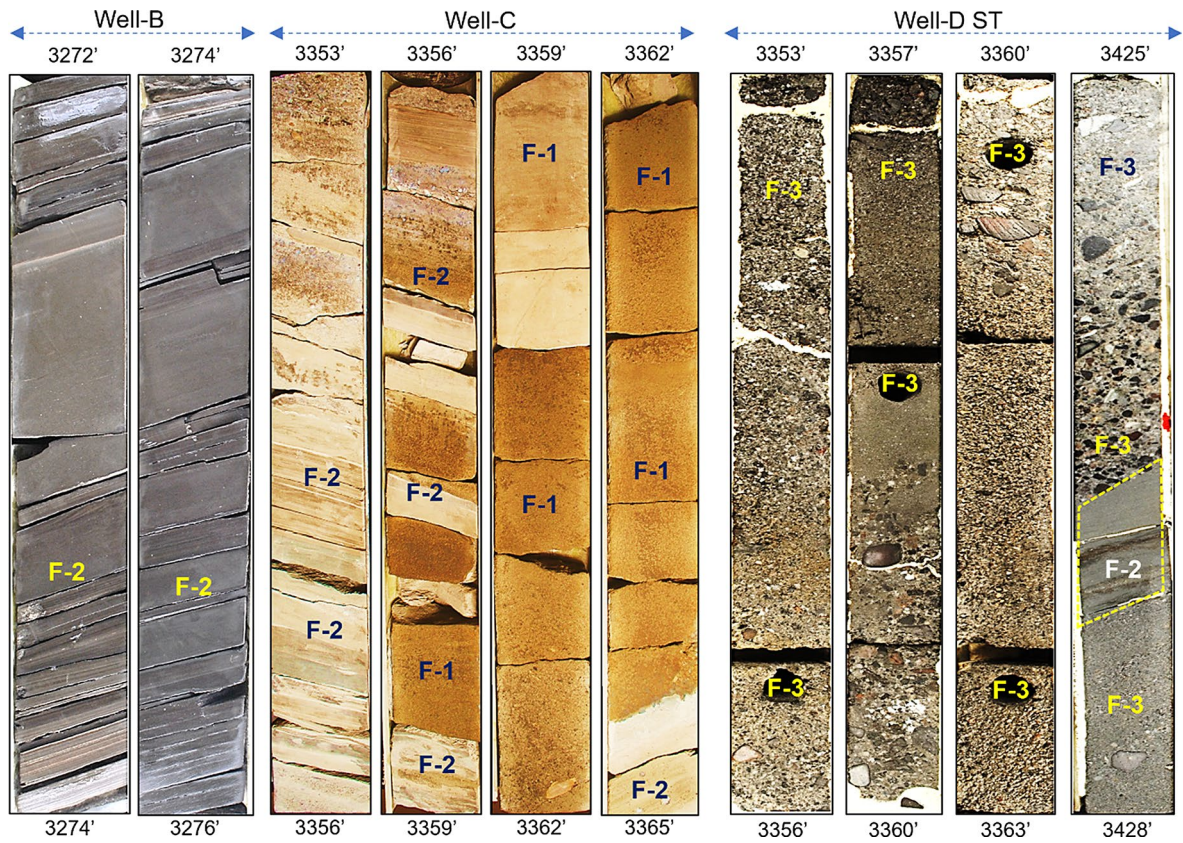
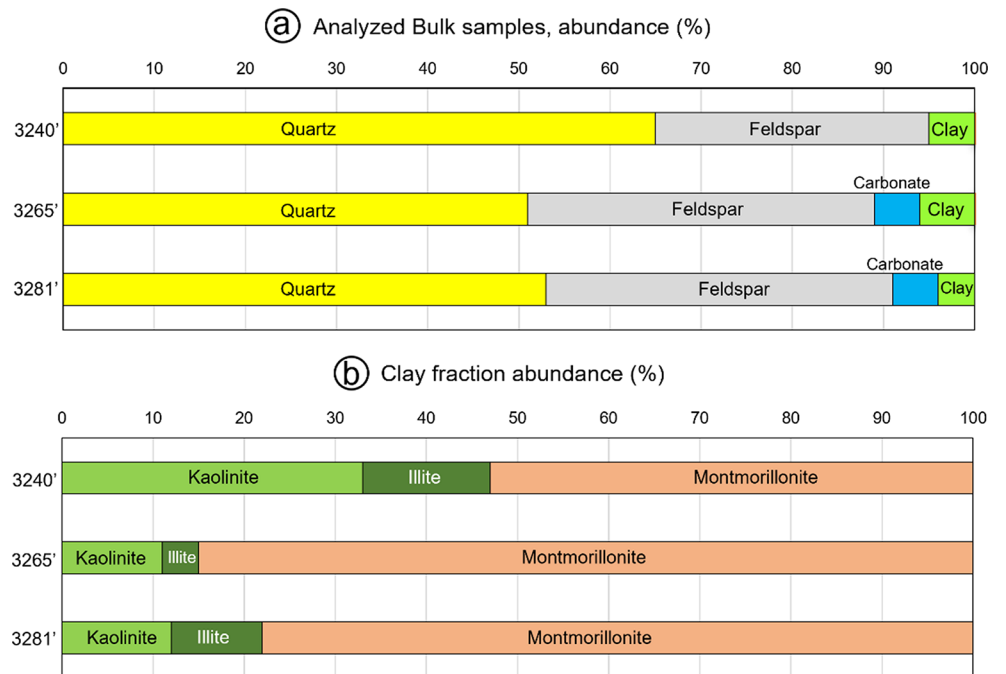


Fig. 4 Core photographs from Well-B, Well-C and Well-D ST indicating the three lithofacies of Hammam Faraun interval: (i) fine to medium-grained massive sandstone (F-1), (ii) low-angle cross-bedded

fine-grained sandstone (F-2) and (iii) coarse to very coarse-grained massive sandstone (F-3)

Fig. 5 XRD results of Hammam Faraun sandstone from Well-B, indicating (a) bulk composition and (b) clay fraction



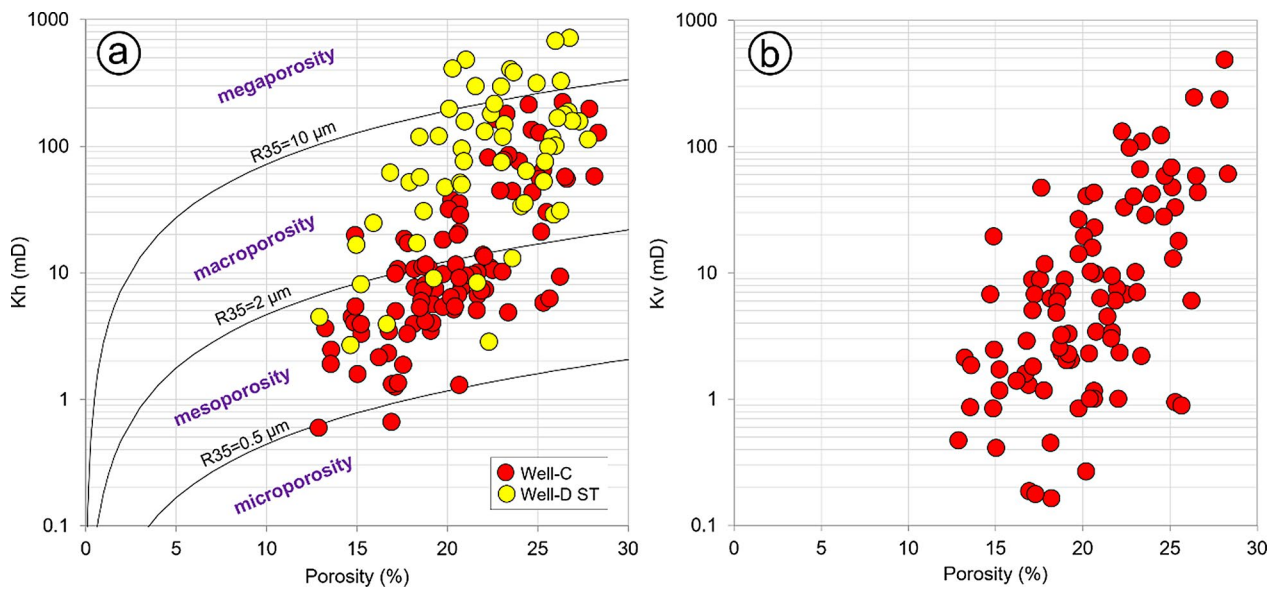


Fig. 6 Cross-plot of core-measured porosity with (a) Kh and (b) Kv of the Hammam Faraun interval from Well-C and Well-D ST. R35 denotes the pore throat radius (Kolodzie 1980)

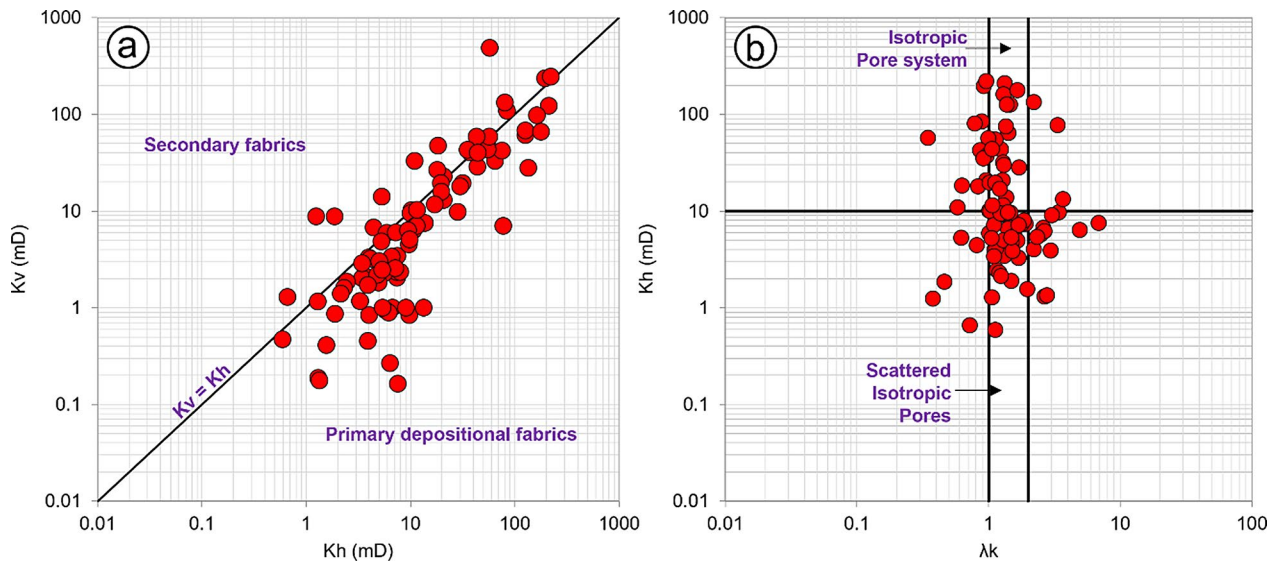


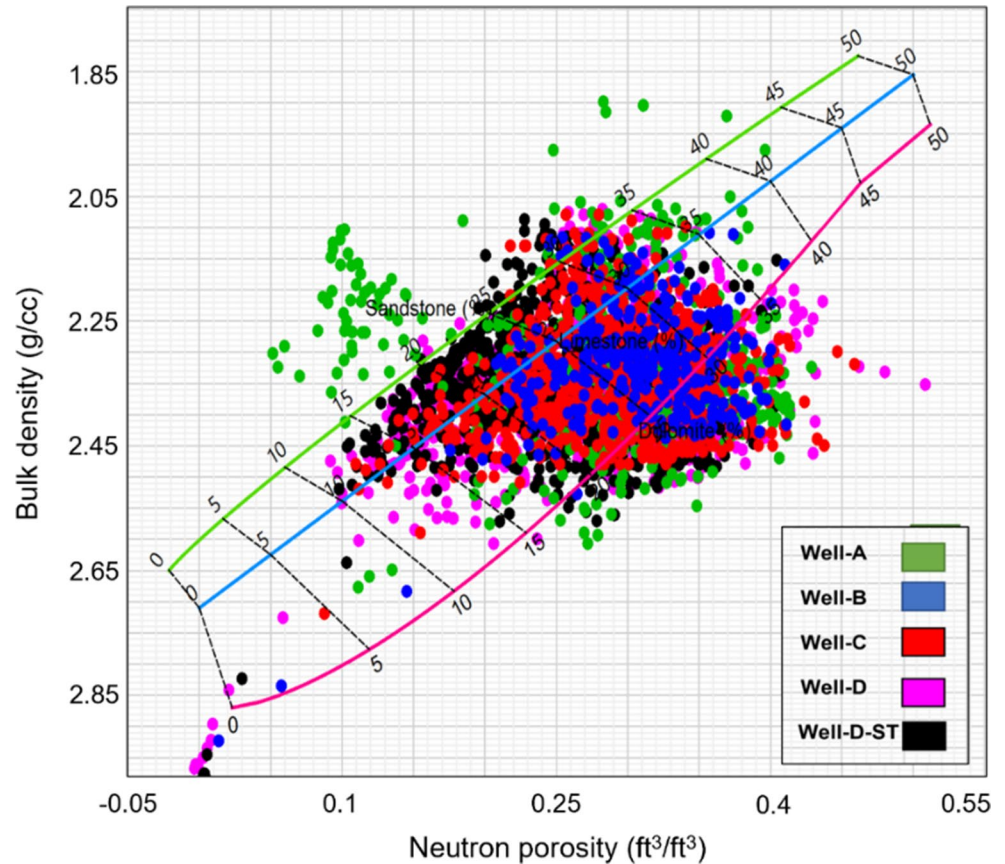
Fig. 7 Cross-plot between (a) horizontal permeability (Kh) and vertical permeability (Kv), (b) permeability anisotropy (λk) and Kh, from Hammam Faraun interval, Well-C

485 mD (Fig. 6b), with majorly $Kv/Kh < 1$ indicating the predominance of primary depositional fabric over secondary fabrics (Fig. 7a). Permeability anisotropy of the studied interval in Well-C ranges between 0.34 and 6.81, however majority of the data distribution indicates $1 < \lambda k < 2$, indicating dominantly isotropic pore system (Fig. 7b). Minor horizontal and vertical pore communication (scattered or connected) is also observed based on the λk -Kh cross-plot.

Wireline log-based petrophysical analysis

Wireline logs of the five studied wells were interpreted for the formation evaluation of the Hammam Faraun interval. For lithological and mineralogical interpretation, we generated the cross-plots between bulk density and neutron porosity (Fig. 8), M and N (Fig. 9) and apparent matrix density vs. apparent matrix volumetric photoelectric factor (Fig. 10). The RHOB-NPHI cross-plot indicates most of the data distribution between the sandstone and dolomite lines with porosity tentatively between 10 and 35%. It is to be noted that the plot represents the entire Hammam Faraun

Fig. 8 Cross-plot between bulk density and neutron porosity of the Hammam Faraun interval of the five studied wells indicating the lithological composition

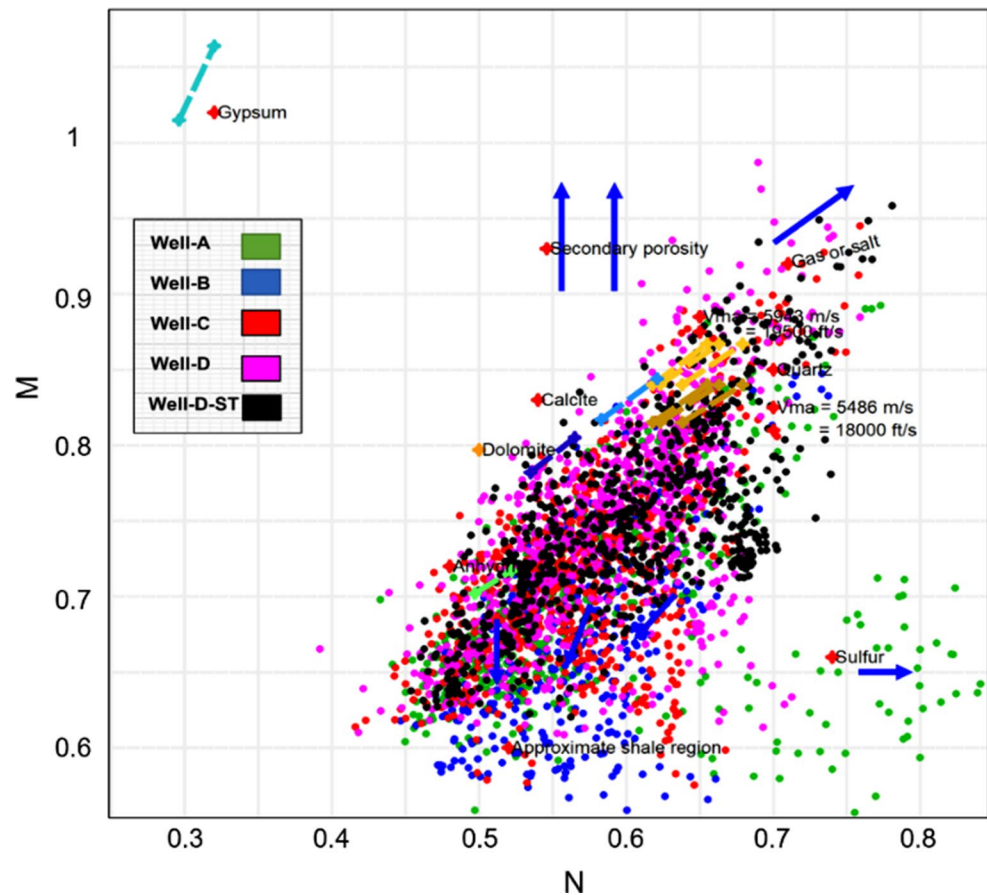


intervals of the studied wells. The effect of limestone and dolomite seen in Fig. 1 may be representative of the calcareous nature of the Hammam Faraun sandstones. This inference does not contradict the observed sandstone cores and the presence of carbonates observed from the XRD measurements in Well-B. The M-N cross-plot in Fig. 11 facilitated the differentiation between shale and sand intervals. The cross-plot indicated the dominance of sandstone lithologies in the Hammam Faraun interval with silica (Quartz), calcite and dolomite to be the major mineralogy. The effect of secondary porosity was not observed in Fig. 11. For matrix identification, the RHOMAA-UMAA cross-plot is presented in Fig. 12. Based on the large data scatter, any specific matrix type could not be inferred, however, it shows the presence of quartz, feldspar, calcite, dolomite, and some clay minerals. All three cross-plots along with the sandstone cores and XRD measurements indicate arkose to calcareous arkose nature of the Hammam Faraun interval.

The quantitative petrophysical interpretations from wireline logs of the five studied wells are presented in Figs. 13, 14, 15, 16 and 17. In Well-A, two promising zones were observed between 2715 and 2770 m and 2850–2890 m, separated by a thick shale-dominated interval. These two intervals contribute to 40.5 m of net pay out of 49.5 m net sand thickness and 248.8 m gross thickness of Hammam

Faraun Member (net to gross ratio of 0.16) with an average $V_{sh} \sim 0.1$ v/v, porosity ~ 0.24 v/v and $Sw \sim 0.33$ v/v (Fig. 13). Well-B exhibits hydrocarbon-bearing zones between 3175 and 3220 m and 3250–3315 m, contributing to 75 m net sand thickness and 15 m net pay (net to gross ratio of 0.09) with an average $V_{sh} \sim 0.2$ v/v, porosity ~ 0.21 v/v and $Sw \sim 0.41$ v/v (Fig. 14). The Hammam Faraun Member has a 350 m thickness in Well-C with a net sand thickness of 219 m. Based on the petrophysical cutoffs, a 20.5 net pay is identified between 3350 and 3500 m in Well-C with an average $V_{sh} \sim 0.12$ v/v, porosity ~ 0.22 v/v and $Sw \sim 0.49$ v/v (Fig. 15). Well-D exhibits hydrocarbon-bearing interval between 3400 and 3465 m with a net pay thickness of 62.5 m, characterized by an average $V_{sh} \sim 0.3$ v/v, porosity ~ 0.18 v/v and $Sw \sim 0.49$ v/v (Fig. 16). Well-D ST shows 43 m of net pay zone between 3375 and 3485 m with an average $V_{sh} \sim 0.18$ v/v, porosity ~ 0.18 v/v and $Sw \sim 0.43$ v/v (Fig. 17). A comparison of the key petrophysical parameters from the five studied wells is presented in Fig. 18. All the upscaled petrophysical properties are populated across the field to understand the lateral distribution of reservoir parameters, as presented in Figs. 19 and 20. Briefly, the area between Well-B and Well-C shows the potential of lower V_{sh} and Sw along with higher effective porosity, net sand, and net pay thickness.

Fig. 9 Cross-plot between M and N of the Hammam Faraun interval of the five studied wells indicating the mineralogical composition



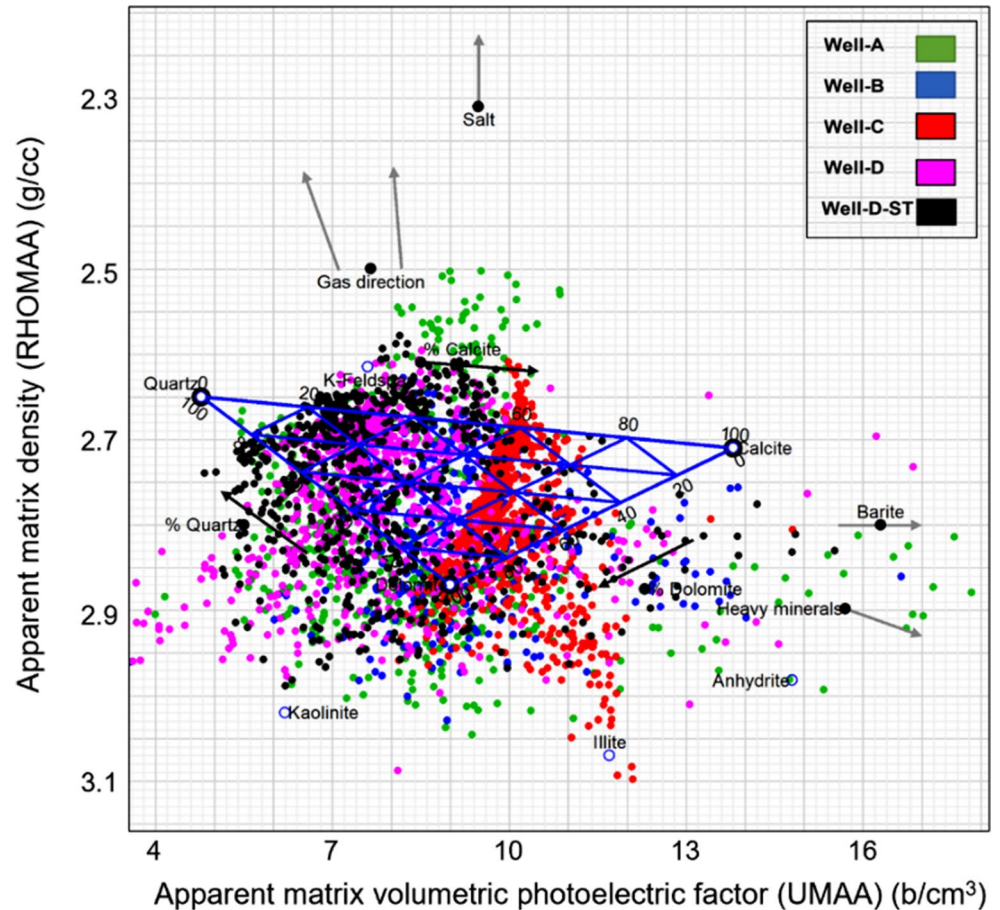
Gas chromatography analysis

Gas chromatograph data from mudlogging services was assessed to estimate various gas ratios which are helpful to indicate possible hydrocarbons present within the studied Hammam Faraun reservoirs. Two wells (Well-C and Well-D) are studied, and the results are presented in Figs. 19 and 20. Between 3355 and 3455 m in Well-C, gas data shows hydrocarbon-bearing zones with majorly Wh > Bh with Wh ~ 17–60 and Bh ~ 2–10 (Fig. 19). The corresponding Ch > 0.5 indicates the presence of liquid hydrocarbon. The estimated OI varies between 0.02 and 0.56 (Fig. 19). Most data show $0.1 < OI < 0.4$ indicating oil, while some data point exhibits $0.07 < OI < 0.1$ which is indicative of condensate or light oil with gas oil ratio (GOR). All the gas ratios point towards oil-bearing intervals between 3355 and 3455 m in Well-C, which is also supported by the estimated Sw (refer to Fig. 15). The gas data in Well D exhibits hydrocarbon bearing zone between 3400 and 3550 m with Wh > Bh, Wh ~ 30–50, Bh ~ 1.2–4, Ch > 0.5 and OI mostly between 0.1 and 0.4, indicating the presence of oil. The same interval also exhibits low Sw in the quantitative petrophysical analysis (Fig. 16).

Discussions

The studied Hammam Faraun Member hosts oil-bearing, porous, and permeable, calcareous arkose, as inferred from the integrated assessment of core analysis, wireline logs, and gas chromatograph data. The studied interval was deposited during the Middle Miocene syn-rift stage. El-Naby et al. (2016) reported that the facies distribution of the syn-depositional Miocene sediments was guided by the structural framework of the southern GOSB, where the sedimentation occurred on the tilted pre-rift blocks. During the deposition of the Belayim Formation, the subsidence rate decreased (El-Naby et al. 2016). Naggar and El-Hilaly (1985) and El-Naby et al. (2016) indicated that the evaporite dominated Belayim Formation was deposited in a closed lagoonal setup with clastic influx episodes. Based on the spectral gamma ray logs, Nabawy and El Sharawy (2015) inferred a lagoonal/shallow marine to continental depositional environment for the Hammam Faraun Member in the southern GOS. The sand fraction of the Hammam Faraun Member increases towards the basin margin part, where tidal flat to intertidal environment prevailed (Nabawy and El Sharawy 2015). Previous works from other parts of GOS point towards an alluvial fan delta system in a shallow

Fig. 10 Cross-plot between apparent matrix density (RHO-MAA) and apparent matrix volumetric photoelectric factor (UMAA) of the Hammam Faraun interval of the five studied wells indicating the lithological composition



marine setup responsible for the deposition of Hammam Faraun clastics (Ramzy et al. 1996; Hughes et al. 1997; Stephen et al. 2005). Summarily, the previous works indicate towards a basin-ward prograde fan deposit during the high-stand system tract. Our core-based observations also correlate well with such inferences. The massive nature of F-1 and F-3 and lack of any stratification is indicative of rapid deposition in a high discharge depositional environment (Baouche et al. 2020; Sen and Dey 2019, 2020; Leila et al. 2023). The abundant fine to coarse pebbles with various degrees of roundness (subangular to rounded) within F-3 (Fig. 4) also support the inference of a high-energy tidal deposit (e.g., Dey et al. 2018; Dey and Sen 2018; Leila et al. 2023). The massive sands with sharp erosive base and bottom rip-up clasts strongly indicates a high energy channel or fan deposit (Sen et al. 2016; Farouk et al. 2022b; Ali et al. 2023; Leila et al. 2023). Lack of bioturbation, rootlets, and pedogenic features indicate the absence of any sub-aerial exposure during the deposition of all three lithofacies (Dey and Sen 2017; Abdel-Fattah et al. 2022).

Wireline logs provided critical insights on the reservoir characteristics, as the effect of diagenesis reflects on the rock properties captured by the wireline log signatures (e.g., Nabawy 2013; Nabawy et al., 2015, 2020; Safa et al., 2021).

Hammam Faraun Member, along with Sidri Member, is a prolific reservoir of the Belayim Formation in the southern GOS. Nabawy and El Sharawy (2015) inferred very good porosity (13.5–25%) and $S_w \sim 42.3\%$ in the Hammam Faraun clastic unit from the southern GOS. We presented the first routine core analysis of the studied interval from southern GOS. The available direct measurements clearly indicate a superior reservoir quality characterized by meso- to megaporous sandstones with porosity up to 28% and Kh up to 1171 mD. The inference is supported by the quantitative petrophysical interpretation, which indicates $V_{sh} < 0.2$ v/v and $S_w < 0.5$ v/v in all five studied wells. Gas chromatography analysis confirms the presence of liquid hydrocarbons in these intervals. In previous studies, researchers indicated potential hydrocarbon-bearing reservoir intervals in the Matulla, Nukhul and Nubia units of the Esh El Melaha area (Omran et al. 2022b; Elbahrawy et al. 2023), and our study adds the Hammam Faraun reservoir potential, which translates excellent exploration and appraisal opportunities within the Middle Miocene and older stratigraphic succession of the study area.

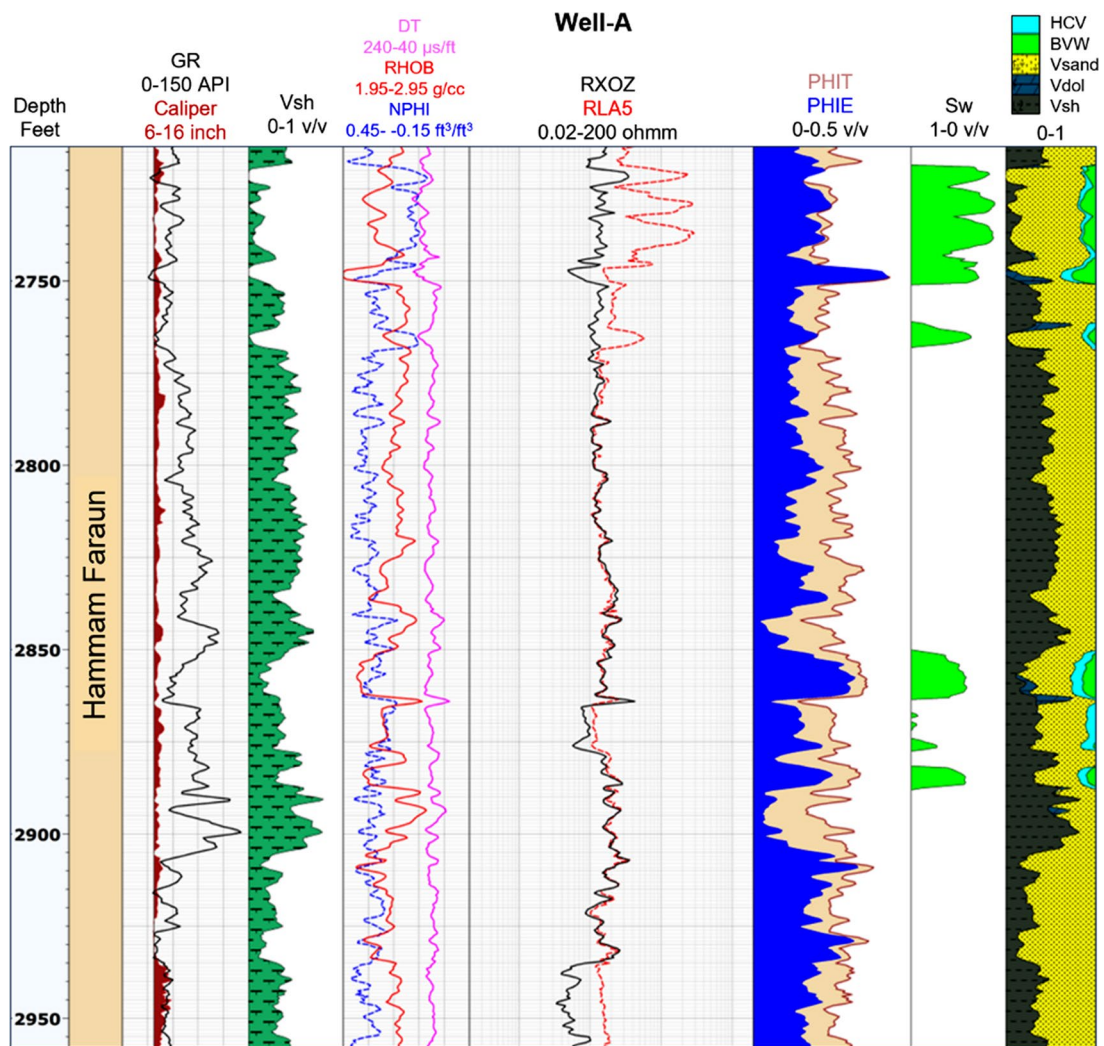


Fig. 11 Petrophysical interpretation of the Hammam Faraun interval in Well-A indicating key petrophysical properties estimated from wireline logs

Conclusions

Integration of core-based lithofacies, XRD, routine core analysis, wireline logs, and mudlogging gas chromatography data shed critical insights on the reservoir characteristics of the Middle Miocene syn-rift Hammam Faraun interval, which are summarised as below:

- The analysed clastic interval is composed of massive medium to coarse-grained massive sandstone and low-angle cross-bedded fine-grained sandstone.
- The sharp erosive base and bottom rip-up clasts of the massive sandstone unit indicate a high energy tidal deposit.

- XRD indicates quartz and feldspar to be the dominant constituents of this calcareous arkose. Montmorillonite is the dominant clay phase.
- Routine core analysis and wireline log-based petrophysical interpretation indicate highly porous and permeable nature of the studied sandstones with $V_{sh} < 0.2$ v/v and $Sw < 0.5$ v/v.
- Various gas ratios (wetness, balance, character, and oil indicator ratio) estimated from the mudlogging chromatograph data indicates the presence of liquid hydrocarbons within the studied reservoirs.

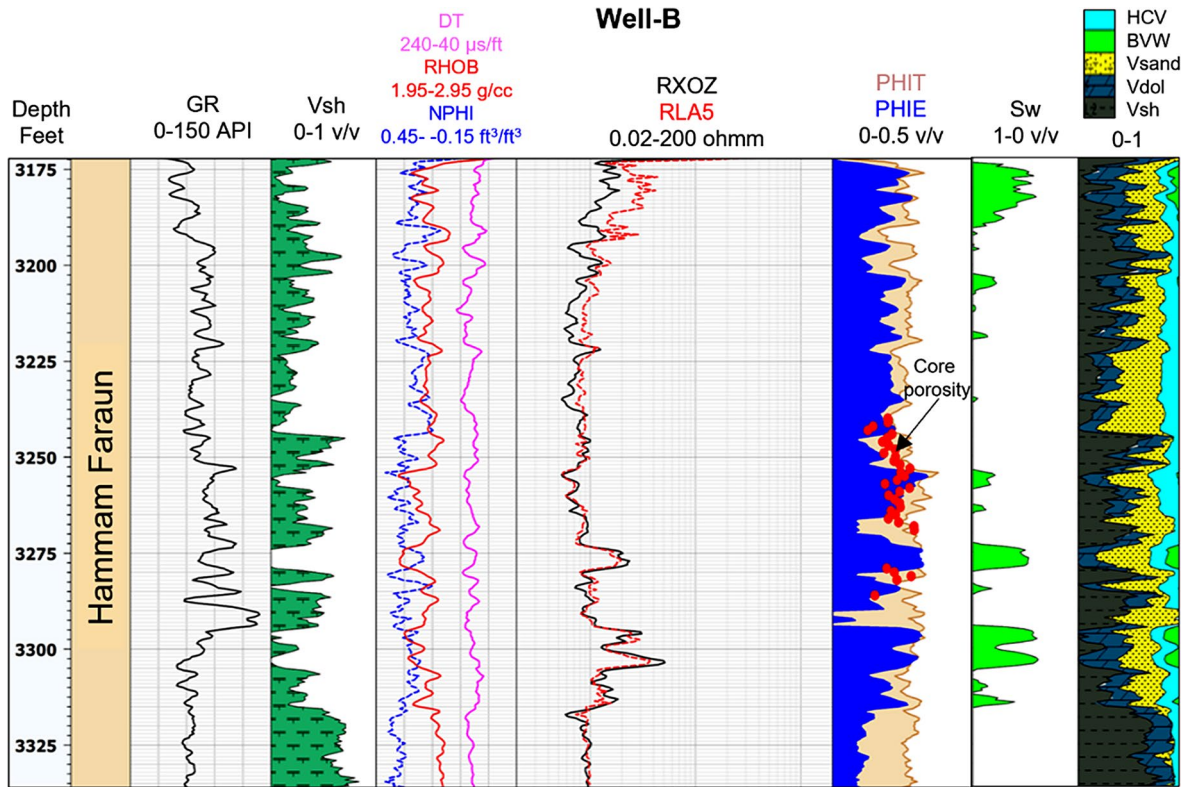


Fig. 12 Petrophysical interpretation of the Hammam Faraun interval in Well-B indicating key petrophysical properties estimated from wireline logs. Red dots on the porosity track represent the helium porosity measurements available from routine core analysis

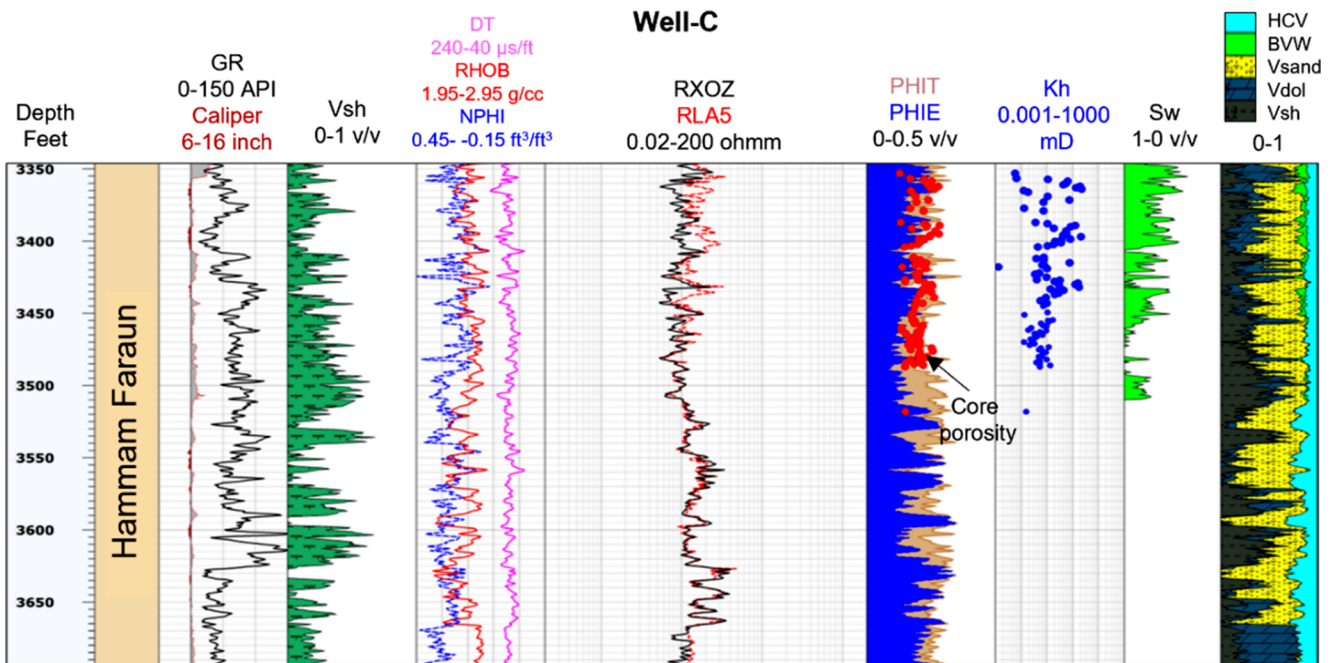


Fig. 13 Petrophysical interpretation of the Hammam Faraun interval in Well-C indicating key petrophysical properties estimated from wireline logs. Red dots on the porosity track represent the helium measurements and blue dots on Kh track represent the horizontal permeability measurements available from routine core analysis

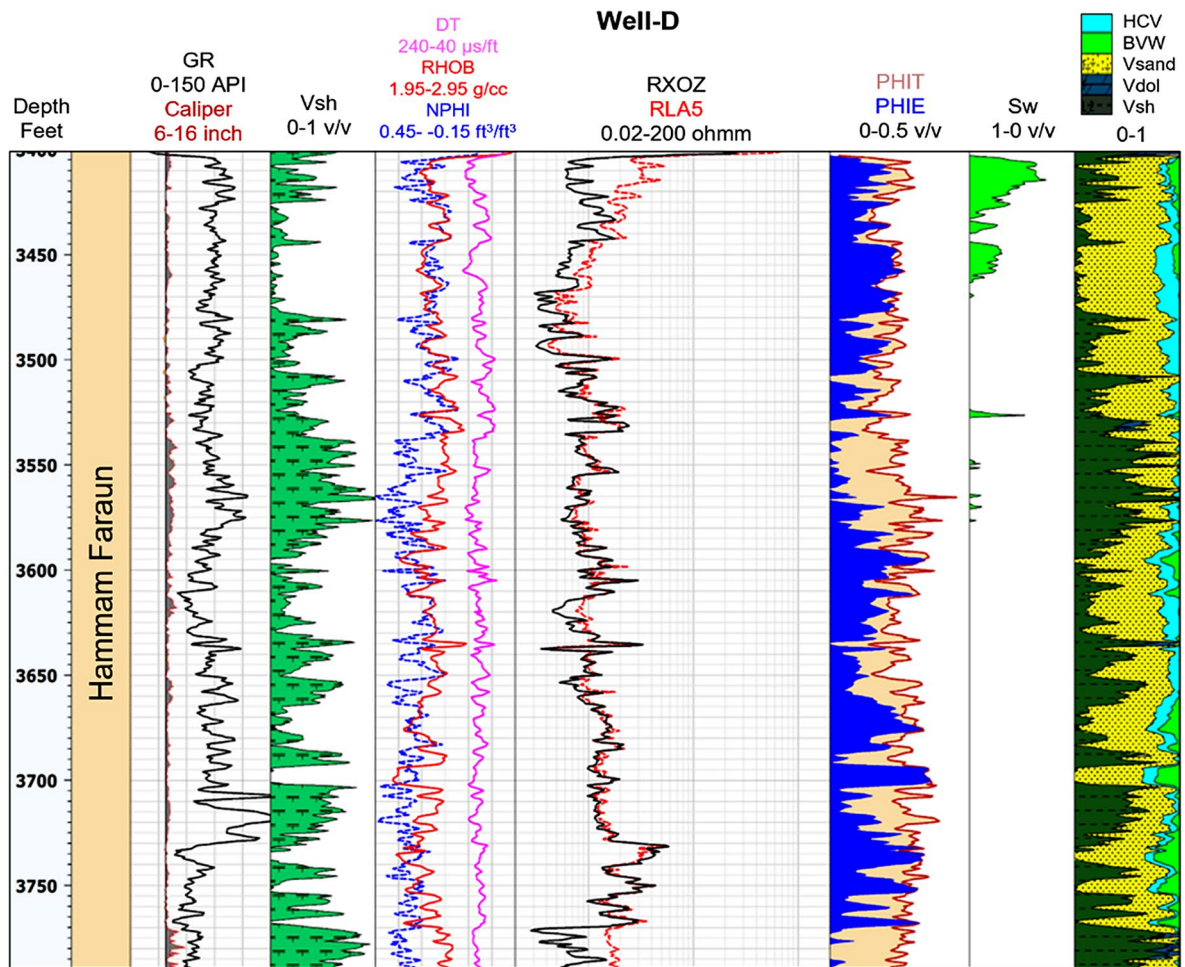


Fig. 14 Petrophysical interpretation of the Hammam Faraun interval in Well-D indicating key petrophysical properties estimated from wireline logs

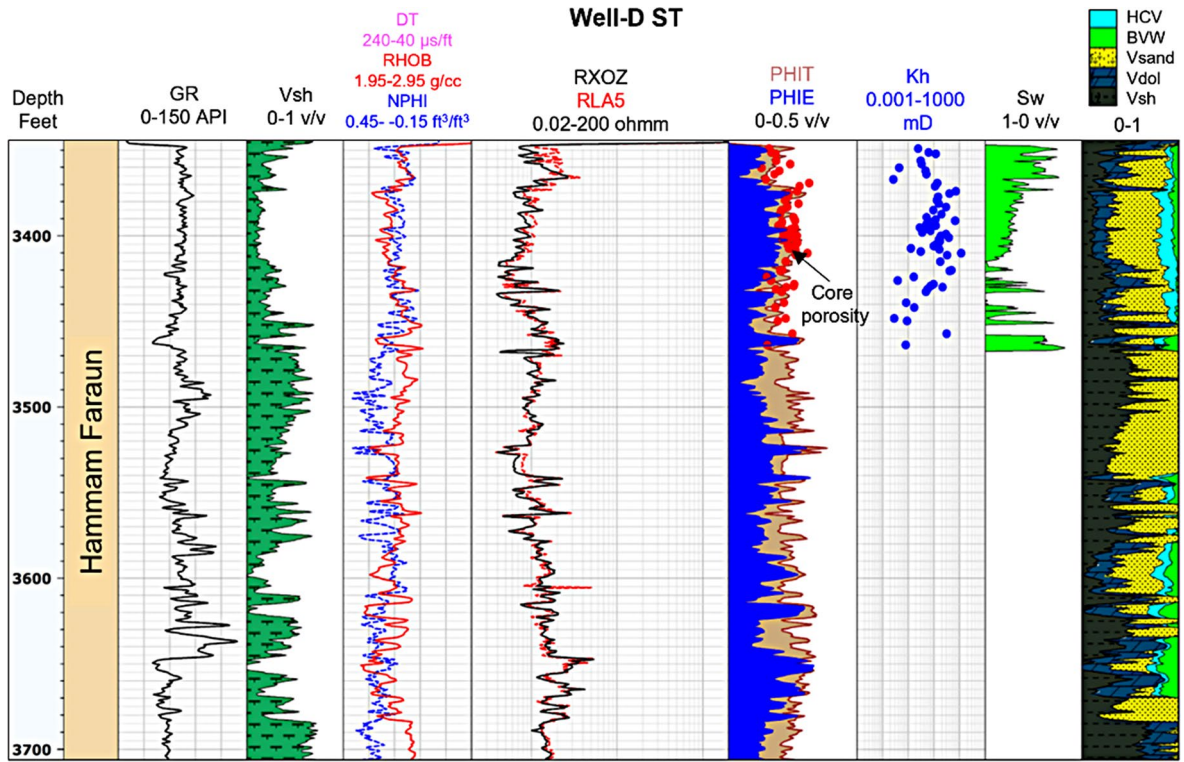
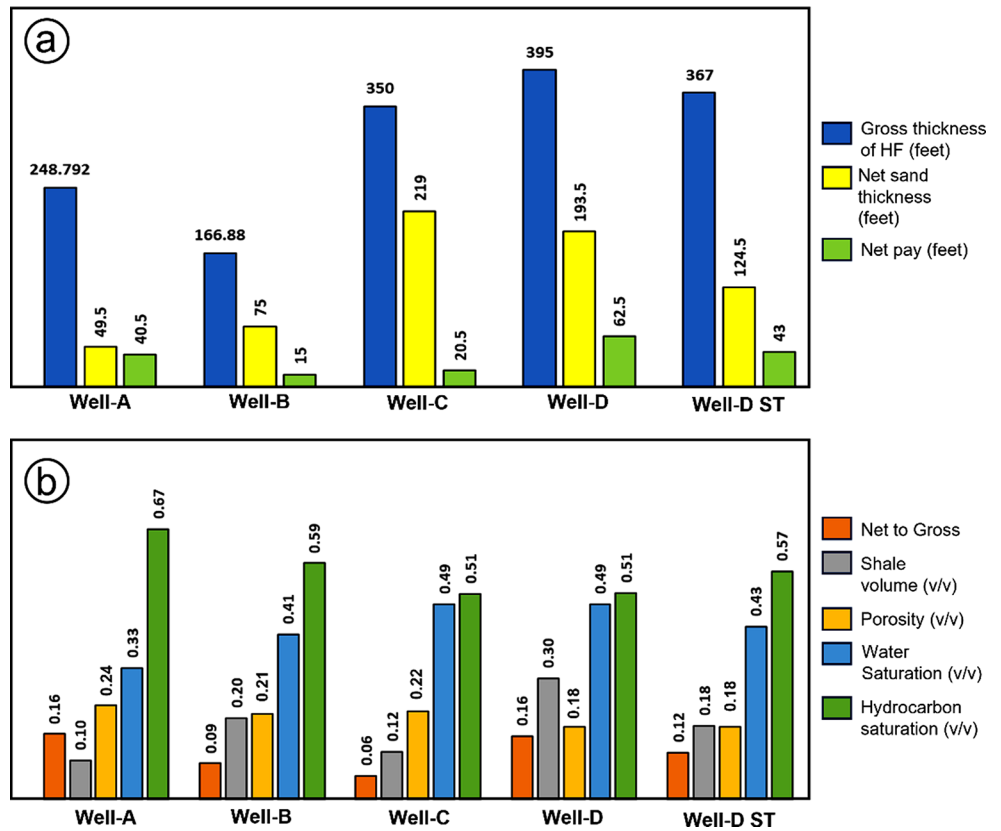


Fig. 15 Petrophysical interpretation of the Hamam Faraun interval in Well-D ST indicating key petrophysical properties estimated from wireline logs. Red dots on the porosity track represent the helium mea-

surements and blue dots on Kh track represent the horizontal permeability measurements available from routine core analysis

Fig. 16 Comparison of key petrophysical properties of the Hamam Faraun Member in the five studied wells that include gross interval thickness, net sand, and net pay thickness along with the average shale volume, porosity, and water/hydrocarbon saturation



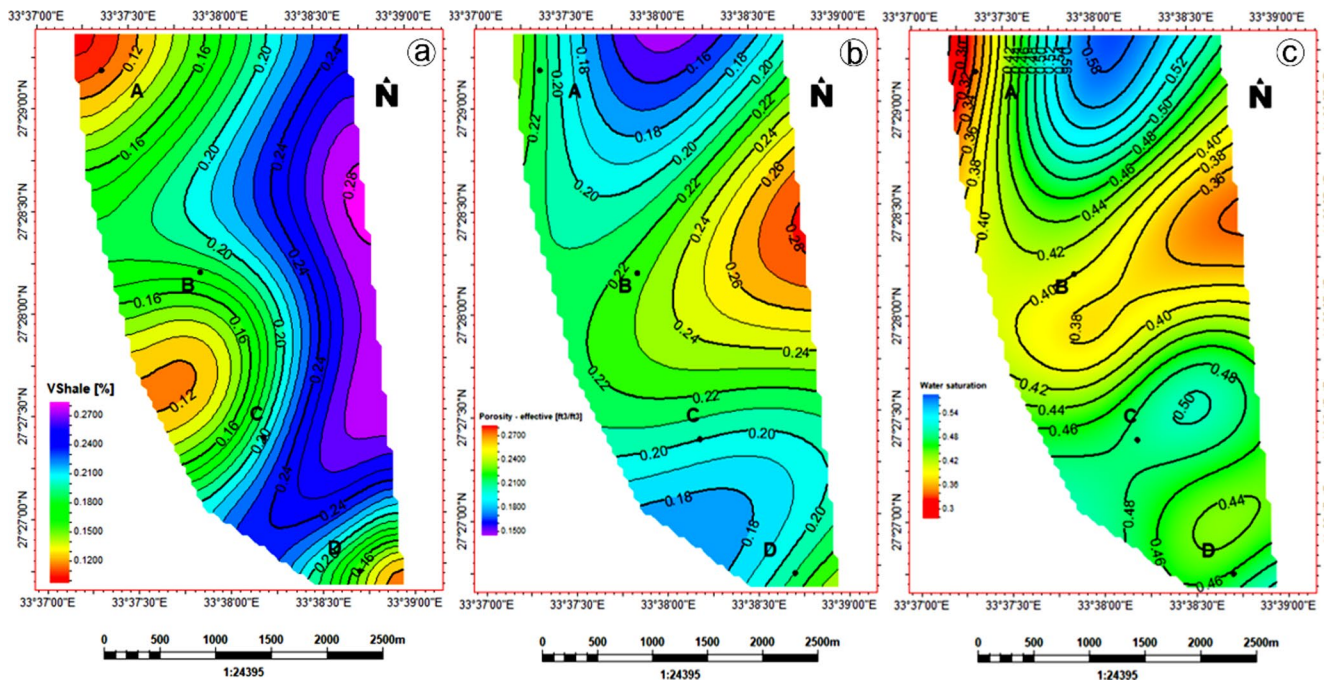


Fig. 17 Distribution of (a) shale volume, (b) effective porosity and (c) water saturation within the Hammam Faraun Member across the study area

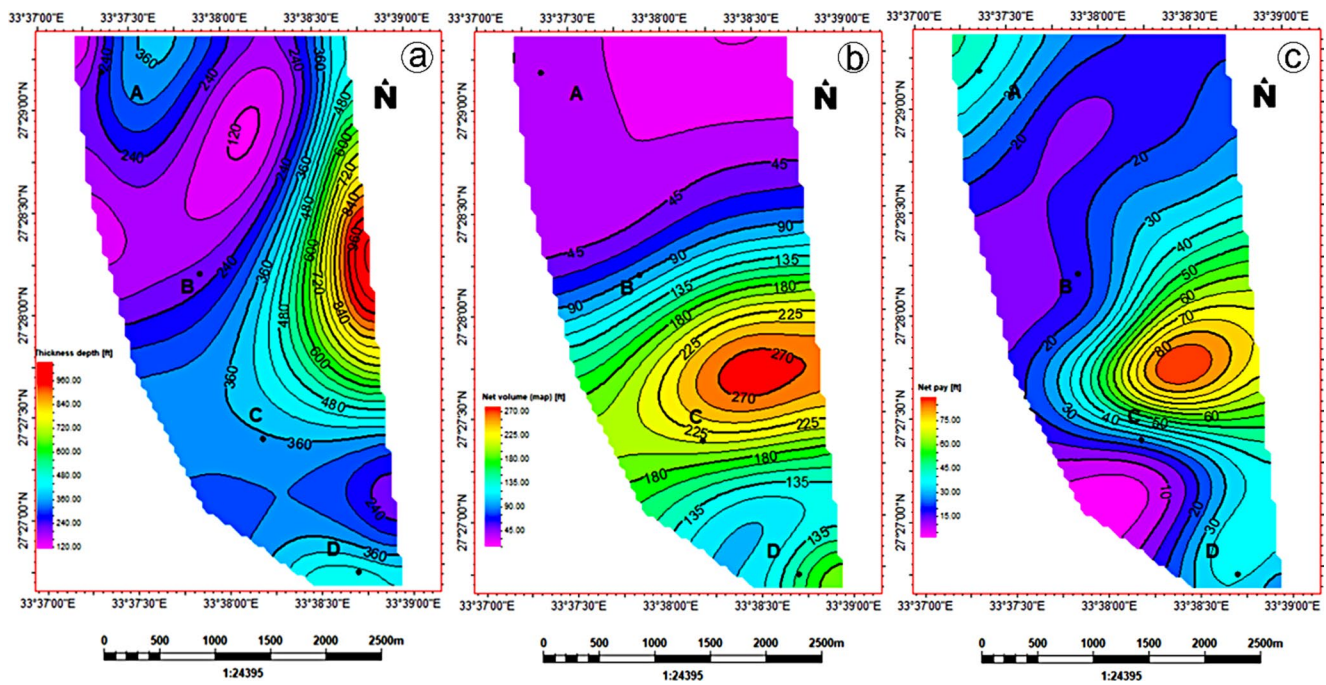


Fig. 18 Distribution of (a) total thickness of Hammam Faraun Member, (b) net sand and (c) net pay across the study area

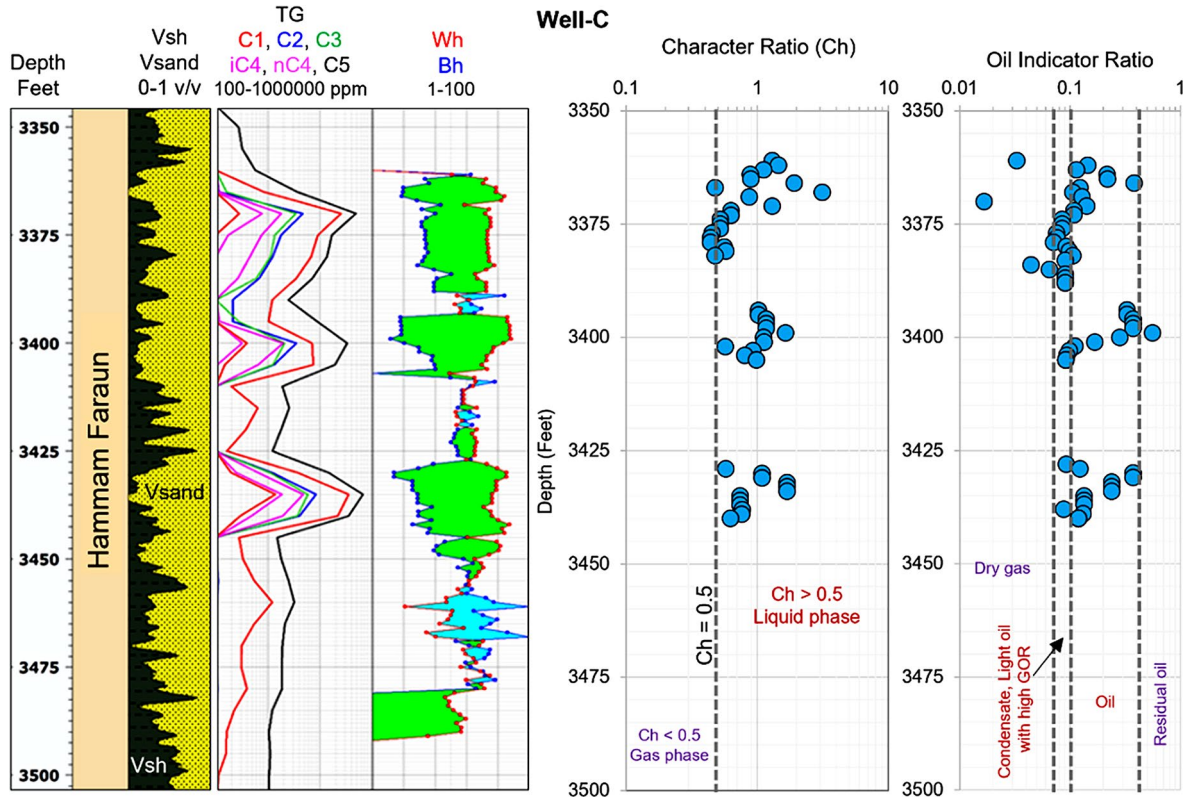


Fig. 19 Gas chromatograph analysis of the Hammam Faraun interval in Well-C indicating possible oil-bearing zones between 3355–3455 m based on gas wetness (Wh), balance (Bh), character (Ch), and oil indicator ratio (OI)

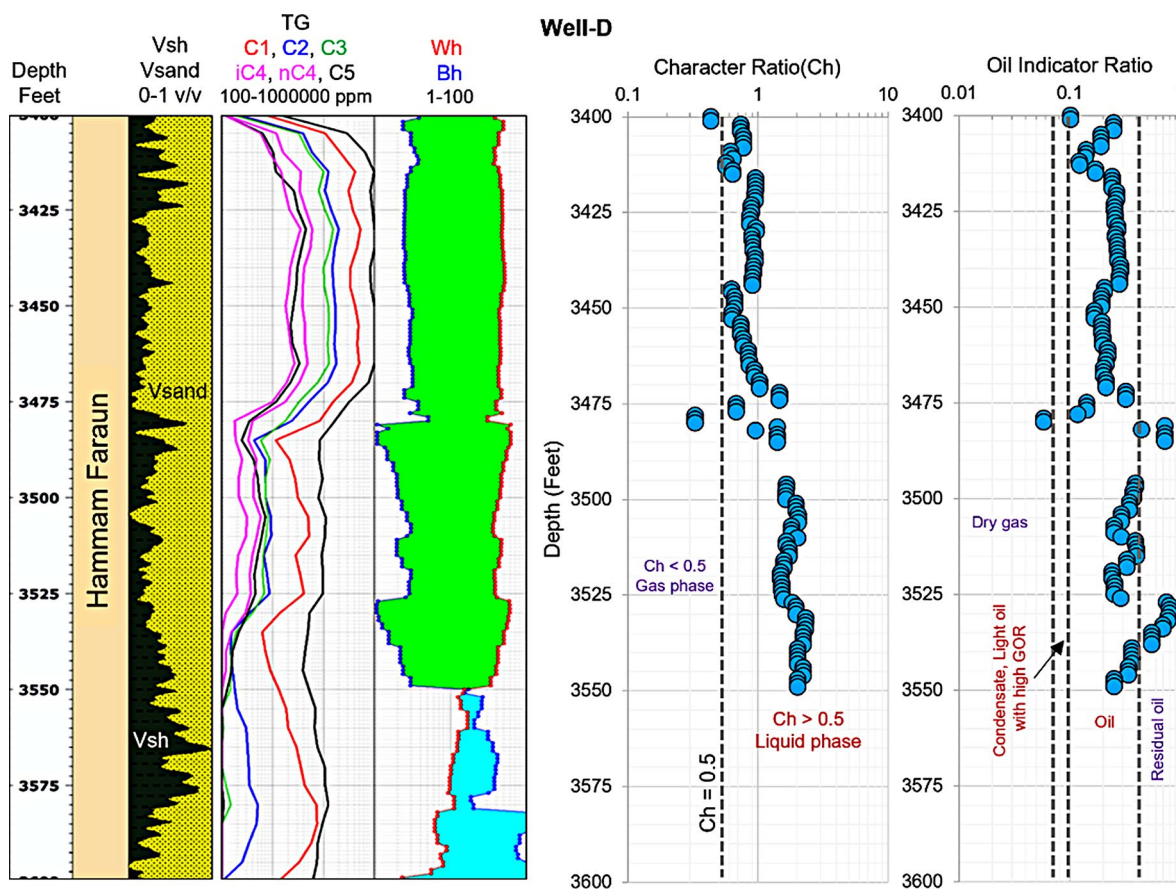


Fig. 20 Gas chromatograph analysis of the Hammam Faraun interval in Well-D indicating possible oil-bearing zones between 3400–3550 m based on gas wetness (Wh), balance (Bh), character (Ch), and oil indicator ratio (OI)

Acknowledgements The authors thank Chun-Feng Li (Editor) for the excellent editorial handling. The two anonymous reviewers are thanked for their constructive review comments which benefited the manuscript. Khaled Al-Kahtany thanks the Research Support Project Number (RSP-2024R139), King Saud University, Riyadh, Saudi Arabia. EGPC is acknowledged for supplying the information utilized in this work.

Author contributions Authors were equally contributed.

Data availability No datasets were generated or analysed during the current study.

Declarations

Competing interests The authors declare no competing interests.

References

Abdel-Fattah MI, Sen S, Abuzied SM, Abioui M, Radwan AE, Bessou M (2022) Facies analysis and petrophysical investigation of the late Miocene Abu Madi sandstone gas reservoirs from offshore Baltim East field (Nile Delta, Egypt). *Mar Pet Geol* 137:105501
 Ali AM, Radwan AE, Abd El-Gawad EA, Abdel-Latif A-SA (2022) 3D Integrated Structural, Facies and Petrophysical Static Modeling Approach for Complex Sandstone Reservoirs: a Case Study

from the coniacian–santonian matulla formation, July Oilfield, Gulf of Suez, Egypt. *Nat Resour Res* 31(1):385–413
 Ali A, Mohamed RSA, Heleika MA, Gabr M, Hashem M, Ahmed MS, Abioui M, Sen S, Abdelhady AA (2023) Evaluation of the Late Messinian Abu Madi sandstone reservoirs in the West Al Khilala gas field, Onshore Nile Delta, Egypt. *Proceedings of the Geologists’ Association*, 135(1), 45–56
 Alsharhan AS (2003) Petroleum geology and potential hydrocarbon plays in the Gulf of Suez rift basin, Egypt. *Rev Am Association Petroleum Geol Bull* 87(1):143–180
 Amer M, Mabrouk WM, Soliman KS, Noureldin AM, Metawally A (2023) Three Dimensional Integrated Geo-Static Modeling for Prospect Identification and Reserve Estimation in the Middle Miocene multi-reservoirs: a Case Study from Amal Field, Southern Gulf of Suez Province. *Nat Resour Res* 32(6):2609–2635
 Asquith G, Gibson C (1982) Basic well log analysis for geologists: methods in Exploration series. AAPG, Tulsa, Oklahoma
 Asquith G, Krygowski D (2004) Basic Well Log Analysis, 2nd.ed. Sections by Steven Henderson and Neil Hurleg. The American Association of Petroleum Geologist, Tulsa, Oklahoma: AAPG Methods in Exploration series, no.16
 Baouche R, Sen S, Debiane K, Ganguli SS (2020) Integrated reservoir characterization of the paleozoic and mesozoic sandstones of the El Ouar field, Algeria. *J Petrol Sci Eng* 194:107551
 Bosworth W, Durocher S (2017) Present-day stress fields of the Gulf of Suez (Egypt) based on exploratory well data: non-uniform regional extension and its relation to inherited structures and local plate motion. *J Afr Earth Sc* 136:136–147

- Bosworth W, Khalil SM, Ligi M, Stockli DF, McClay KR (2020) *Geology of Egypt: the Northern Red Sea. The geology of Egypt.* Springer, Cham, pp 343–374
- Dey J, Sen S (2017) Impact of Bioturbation on Reservoir Quality and production – a review. *J Geol Soc India* 89(4):460–470
- Dey J, Sen S (2018) Sequence Stratigraphic Model of Middle Permian Barakar formation from a marginal Gondwana Basin, India. *J Earth Sci* 29(4):745–754
- Dey J, Sen S, Bhattacharjee S (2018) Geophysical log based coal characterization of middle Permian Barakar formation from North Karanpura coal field, India. *J Geol Soc India* 92:36–44
- El Sharawy MS, Gaafar GR (2012) Application of well log analysis for source rock evaluation in the Duwi formation, Southern Gulf of Suez, Egypt. *J Appl Geophys* 80:129–143
- El Sharawy MS, Nabawy BS (2016) Geological and petrophysical characterization of the Lower Senonian Matulla formation in Southern and Central Gulf of Suez, Egypt. *Arab J Sci Eng* 41:281–300
- El-Naby AA, Younis A, Abd El-Aal M, Alhamsry A (2016) Structures and sequence stratigraphy of the Miocene successions, southwestern Gulf of Suez, Egypt. *J Afr Earth Sc* 117:135–149
- El-Nady MM, Mohamed NS (2016) Source rock evaluation for hydrocarbon generation in halal oilfield, southern Gulf of Suez, Egypt. *Egyptian J Petroleum* 25:383–389
- Elbahrawy A, Omran MA, Khamees H, Sarhan MA (2023) Geophysical structural interpretation of Esh El Mallaha basin, southern Gulf of Suez: implications for oil potential in South Malak and Rabeh fields. *Geomech. Geophys. Geo-Energ. Geo-resour* 9:58
- Elleboudy MM, Sharaf LM, Shahin AN (2011) Hydrocarbon potential and undiscovered reserves in the Southern Gulf of Suez, Egypt. In: *Offshore Mediterranean Conference and Exhibition, Ravenna, Italy, Mar 23–25. OMC-2011-061*
- Elmaadawy KG (2020) Thermal maturity modelling for the pre-miocene source rocks in Ras Garra area, Suez Rift Basin, Egypt. *J Afr Earth Sc* 163:103746
- Elmaadawy KG, Elbassiouny HAM, Raslan SM (2021) Thermal Maturity and Hydrocarbon Generation Modelling for the Lower Rudeis Source Rock and Petroleum System Analysis in Garra Area, South Gulf of Suez, Egypt. *Journal of Petroleum and Mining Engineering* 23(1)
- Farouk S, Sen S, Pigott JD, Sarhan MA (2022a) Reservoir characterization of the middle Miocene Kareem sandstones, Southern Gulf of Suez Basin, Egypt. *Geomech. Geophys. Geo-energ. Geo-resour.* 8, 130
- Farouk S, Sen S, Abuseda H, El-Shamly Y, Salam A, Elhossainy MM (2022b) Petrophysical characterization of the Turonian and Cenomanian intervals in the Abu Gharadig Field, Western Desert, Egypt: inferences on reservoir quality and resource development. *Nat Resour Res* 31:1793–1824
- Folk RL (1980) *Petrology of sedimentary rocks.* Hemphill Publishing Company, Austin, Texas
- Haworth JH, Sellens M, Whittaker A (1985) Interpretation of hydrocarbon shows using light (C1-C5) hydrocarbon gases from mud-log data, vol 69. *The American Association of Petroleum Geologist (AAPG) Bulletin*, pp 1305–1310. 8
- Heidbach O, Tingay M, Barth A, Reinecker J, Kurfeß D, Müller B (2010) Global crustal stress pattern based on the World stress map database release 2008. *Tectonophysics* 482:3–15
- Hughes SC, Ahmed H, Raheem TA (1997) Exploiting the mature South El Morgan Kareem reservoir for yet more oil - a case study in multidiscipline reservoir management. *J Petrol Technol* 49(10):1129–1130 SPE-1097-1129-JPT
- Hussein A, Gamal R, Madi T (2020) Gulf of Suez, Eastern Desert and Sinai: Egypt's Crude Oil Squad [Unpublished report]. *Egypt Oil and Gas Newspaper.* <https://egyptoil-gas.com/reports/gulf-of-suez-eastern-desert-and-sinai-egypts-crude-oil-squad/>
- Hussein IA, Abu-Hashish MF, Elmaadawy K (2024) Geostatic Reservoir modeling of the Kareem formation in GS277 oil field, Gulf of Suez Egypt. *Egyptian J Petroleum* 33(1):9
- Kolodzie S (1980) Analysis of pore throat size and use of the Waxman–Smits equation to determine OOIP in Spindle Field, Colorado. In: *Proceedings Society of Petroleum Engineers, 55th Annual Technical Fall Conference. SPE-9382*
- Leila M, Sen S, Ganguli SS, Moscariello A, Abioui M (2023) Integrated Petrographical and petrophysical evaluation for reservoir management of the Upper Miocene Qawasim sandstones in West Dikrnis, onshore Nile Delta, Egypt. *Geoenergy Sci Eng* 226:211789
- Maestrelli D, Montanari D, Corti G, Del Ventisette C, Moratti G, Bonini M (2020) Exploring the interactions between rift propagation and inherited crustal fabrics through experimental modeling. *Tectonics*, 39, e2020TC006211.
- Meshref WM (1990) Tectonic Framework. In: Said R (ed) *The geology of Egypt.* Balkema, Rotterdam, pp 113–155
- Meshref W, Eldin SMS, Refai E, Abdelhady YE, Hammouda H (1995) Southern Gulf of Suez: Rift Tectonics. In: Ojankangas, R.W., Dickas, A.B., Green, J.C. (eds) *Basement Tectonics 10. Proceedings of the International Conferences on Basement Tectonics*, vol 4. Springer, Dordrecht. https://doi.org/10.1007/978-94-017-0831-9_45
- Mode AW, Anyiam OA, Egbujie BC (2014) The Application of Chromatographic Gas Ratio Analysis in Reservoir Fluid evaluation of Beta Field in the Congo Basin. *J Geol Soc India* 84:303–310
- Moustafa AR (1993) Structural characteristics and tectonic evolution of the east margin blocks of the Suez rift. *Tectonophysics* 223:381–399
- Nabawy BS (2013) Impacts of dolomitization on the petrophysical properties of El-Halal formation, North Sinai, Egypt. *Arab J Geosci* 6(2):359–373
- Nabawy BS (2018) Impacts of the fossil anisotropy on the electric and permeability anisotropy of the highly fossiliferous limestone: a case study. *Mar Geophys Res* 39(4):537–550
- Nabawy BS, Al-Azazi NA (2015a) Reservoir zonation and discrimination using the routine core analyses data: the upper jurassic Sabatayn sandstones as a case study, Sabatayn basin, Yemen. *Arab J Geosci* 8(8):5511–5530
- Nabawy BS, El Sharawy MS (2015) Hydrocarbon potential, structural setting and depositional environments of Hamma Faraun Member of the Belayim formation, Southern Gulf of Suez, Egypt. *J Afr Earth Sc* 112:93–110
- Nabawy BS, Sediek KN, Nafee SA (2015b) Pore fabric assignment using the electrical conductivity of some albian–cenomanian sequences in North Eastern Desert, Egypt. *Arabian J Geosci* 8(8):5601–5615
- Nabawy BS, Mansour AS, Rashed MA, Afify WSM (2020) Implementation of sedimentary facies and diagenesis on the reservoir quality of the Aquitanian–Burdigalian Rudeis formation in the Gulf of Suez, Egypt: a comparative surface and subsurface study. *Geological J* 55(6):4543–4563
- Naggar AA, El-Hilaly H (1985) Geological aspects and reservoir units of Ras Budran field. *Egyptian General Petroleum Corporation, 8th production seminar. Egypt*, pp 1–12
- Omran MA, El Sharawy MS (2014) Tectonic evolution of the Southern Gulf of Suez, Egypt: a comparison between depocenter and near peripheral basins. *Arab J Geosci* 7:87–107
- Omran MA, Assal EM, Raia MAA, Sarhan MA (2022a) Oil potentialities of West Esh El-Mallaha area, southern Gulf of Suez as deduced from well log data interpretation. *Sci J Damietta Fac Sci* 13(2):76–83
- Omran MA, Assal EM, Raia MAA, Sarhan MA (2022b) Oil potentialities of West Esh El-Mallaha Area, Southern Gulf of Suez as

- deduced from well log data interpretation. *Sci J Damietta Fac Sci* 13(2):76–83
- Patton TL, Moustafa AR, Nelson RA, Abdine SA (1994) Tectonic evolution and structural setting of the Suez rift. In: Landon SM (ed) *Interior Rift basins*, vol 59. American Association of Petroleum Geologists Memoir, pp 9–55
- Pierson RM (2017) The ELLA GRA process - concepts and methods for the prediction of Reservoir Hydrocarbon Type using ratios of gas chromatography C1-C5 gases. AAPG Rocky Mountain section meeting, billings, Montana, June 25–28. Search and Discovery Article #42122.
- Poupon A, Leveaux J (1971) Evaluation of water saturation in shaly formations. *Log Anal* 12(04):SPWLA-1971
- Radwan AE, Abdelghany WK, Elkhawaga MA (2021) Present-Day in-situ stresses in Southern Gulf of Suez, Egypt: insights for stress rotation in an extensional rift basin. *J Struct Geol* 147:104334
- Ramzy M, Steer B, Abu-Shadi F, Schlorholtz M, Mika J, Dolson J, Zinger M (1996) Gulf of Suez basin sequence models-part B. Miocene sequence stratigraphy and exploration significance in the central and the southern Gulf of Suez. In: EGPC 13th Exploration Conference, Cairo, Egypt, vol. 2, 242–256
- Safa MG, Nabawy BS, Basal AMK, Omran MA, Lashin A (2021) Implementation of a Petrographical and Petrophysical Workflow Protocol for studying the impact of heterogeneity on the Rock typing and Reservoir Quality of Reefal Limestone: a Case Study on the Nullipore carbonates in the Gulf of Suez. *Acta Geologica Sinica (English Edition)* 95(5):1746–1762
- Said R (1990) *The geology of Egypt*. Elsevier, New York, p 734
- Selim ES, Sarhan MA (2024) Petrophysical evaluation of the pre-rift hydrocarbon reservoirs in the Gulf of Suez Basin. *Egyptian J Petroleum* 33(1):10
- Sen S, Dey J (2019) A field-scale overview of facies architectures and depositional environment integrating core and geophysical log data: study from a marginal Gondwana Basin, India. *J Geol Soc India* 94(3):238–244
- Sen S, Dey J (2020) Cyclic sedimentation in the Barakar formation of the Karanpura Field, marginal Gondwana Basin, India. *J Geol Soc India* 95:293–300
- Sen S, Das N, Maiti D (2016) Facies analysis and depositional model of late Permian Raniganj formation: study from Raniganj Coal bed methane block, India. *J Geol Soc India* 88(4):503–516
- Stephen RP, Michael TA, Charles RB, William BM, David JR, David MS, Mark VW (2005) Preferential deposition and preservation of structurally-controlled synrift reservoirs: Northeast Red Sea and Gulf of Suez. *GeoArabia* 10(1):97–124
- Van Dijk J, Ajayi AT, De Vincenzi L, Ellen H, Guney H, Holloway P, Khdaouria M, Mcleod IS (2020) Hydrocarbon Exploration and Production Potential of the Gulf of Suez Basin in the Framework of the New Tectonostratigraphic Model. International Petroleum Technology Conference, Dhahran, Kingdom of Saudi Arabia, Jan 13–15. IPTC-19810-MS
- Younes AI, McClay K (2002) Development of accommodation zones in the Gulf of Suez-Red Sea rift. *Egypt Am Assoc Pet Geol Bull* 86:1003–1026

Publisher's Note Springer Nature remains neutral with regard to jurisdictional claims in published maps and institutional affiliations.

Springer Nature or its licensor (e.g. a society or other partner) holds exclusive rights to this article under a publishing agreement with the author(s) or other rightsholder(s); author self-archiving of the accepted manuscript version of this article is solely governed by the terms of such publishing agreement and applicable law.